ACS APPLIED MATERIALS & INTERFACES

RESEARCH ARTICLE

www.acsami.org

Resistive Switching Behavior and Multiple Transmittance States in Solution-Processed Tungsten Oxide

Wei-Ting Wu,[†] Jih-Jen Wu,[‡] and Jen-Sue Chen*[,†]

[†]Department of Materials Science and Engineering, National Cheng Kung University, Tainan 701, Taiwan

[‡]Department of Chemical Engineering, National Cheng Kung University, Tainan 701, Taiwan

Supporting Information

ABSTRACT: In this work, a tungsten oxide (WO_x) film is prepared using a thiourea-assisted solution process. We demonstrate a device composed of fluorine doped tin oxide (FTO)-glass/WO_x/electrolyte/indium-tin oxide (ITO)-glass stacking electrochromic (EC) structure and Al electrodes that are locally patterned and interposed between the WO_x film and electrolyte, which form an Al(top electrode)/WO_x/FTO(bottom electrode) resistance random access memory (RRAM) unit. According to transmission electron microscopy and X-ray photoelectron spectroscopy analyses, the WO_x film contains nanosize pores and metallic-tungsten nanoclusters which are scattered within the tungsten oxide layer and concentrated along the interface between the Al electrode and WO_x film. With application of voltage to the ITO electrode, multiple transmittance states are achieved for the EC unit due to the different quantity of intercalated Li ions in the WO_x film. As for the Al/WO_x/FTO RRAM unit, a bipolar nonvolatile resistive switching behavior is attained by applying voltage on the Al top electrode, showing electrical bistability with an ON/OFF current ratio up to 1×10^4.

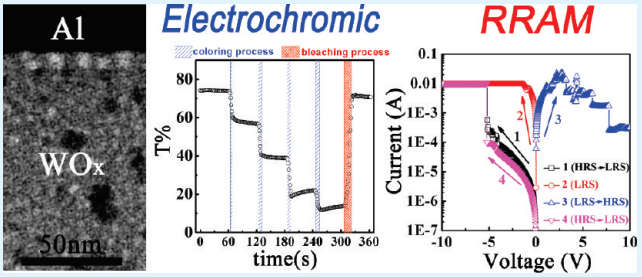

KEYWORDS: tungsten oxide, electrochromic, multiple transmittance states, resistive switching, nonvolatile memory, optical memory

1. INTRODUCTION

Tungsten oxide has demonstrated several potential applications, including electrochromic (EC) devices,[1−3] gas sensors,[4] and photocatalysts,[5] etc. As one of the most studied cathodic EC materials, the color of tungsten oxide switches from transparent to blue upon intercalation of lithium ions (Li^+) or protons (H^+).[1−3] General applications of EC devices include smart windows,[6] mirrors,[7] and eyewear.[8] In addition, Sonmez et al.[9] and de Ruiter et al.[10] have demonstrated EC polymeric memory devices with recording states based on variations in optical density. The colored/bleached states of EC devices are analogous to memory states in data storage devices.

On the other hand, many transition metal oxides, such as NiO,[11,12] TiO_2,[13,14] WO_3,[15,16] SiO_2,[17] $SrTiO_3$,[18] and $La_{0.7}SrMn_{0.3}O_3$,[19] have been reported their resistive switching behavior in a metal/insulator/metal (MIM) structure. The resistive switching character constitutes the data recording mechanism of resistance random access memory (RRAM), which is an emerging category of nonvolatile memories (NVM) due to its simple structure, high integration density, high speed and low power consumption.[20] Although tungsten oxide is not the most investigated transition metal oxide for RRAM, Ho et al.[15] have reported a 9 nm half-pitch tungsten oxide based RRAM cell fabricated using the nanoinjection lithography technique. The minute pitch size potentially allows the fabrication of high-density memory; however, the delicate nanoinjection lithography technique inevitably increases the process complexity and decreases the throughput.[13,15]

In this study, we investigate the EC and resistive switching properties of a solution-derived tungsten oxide (WO_x) film in a composite device comprised of EC and RRAM units. The composite device is fabricated on a fluorine doped tin oxide (FTO)-glass substrate with the WO_x film spin-coated on top. The EC unit is constituent of an FTO-glass/WO_x/electrolyte/indium−tin oxide (ITO)-glass stack and the RRAM units are constructed by locally interposing patterned Al electrodes between the WO_x film and electrolyte to form the Al(top electrode)/WO_x/FTO(bottom electrode) MIM structure. Here the WO_x film synthesized via a thiourea-assisted route[3] is composed of nanosized pores and metallic-tungsten nanoclusters embedded in the tungsten oxide matrix. Transmittances of porous WO_x film in the EC units are controlled by the quantity of intercalated Li ions. The Al/WO_x/FTO RRAM unit exhibits bipolar resistive switching behavior with an ON/OFF current ratio up to 1×10^4. Transport of Li ions for modulation of transmittance, as well as and the formation/rupture of conductive paths during resistive switching, shall be associated with the specific microstructure of thiourea-assisted WO_x film and the correlation in between will be explored.

Received: April 8, 2011
Accepted: June 27, 2011
Published: June 27, 2011

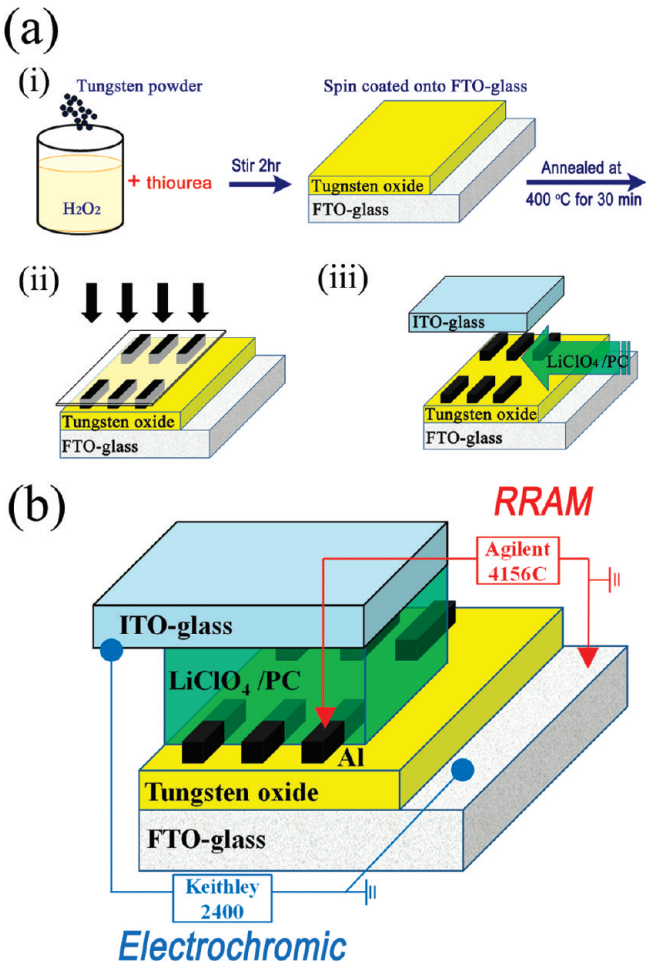

Figure 1. (a) Schematic presentation of WO_x-based device preparation: (i) preparation of WO_x film onto FTO-glass; (ii) sputtering of Al electrodes onto WO_x film; (iii) assembly of device. (b) Schematic diagram of WO_x-based device composed of EC and RRAM units (sizes and thicknesses of the various components are not to scale).

2. EXPERIMENTAL SECTION

Figure 1a shows a schematic diagram of the process flow of preparing the WO_x film and the structure of the WO_x-based device composed of EC and RRAM units. First, the WO_x film was deposited onto FTO coated glass (Solaronix) using the thiourea-assisted method as reported in our previous work[3] (step i in Figure 1a). 1.5 g of tungsten powder (99%, Merck) was dissolved in a mixture of 9 mL of hydrogen peroxide (30%, Sigma-Aldrich) and 1 mL of deionized water to form the peroxopolytungstic acid (PTA) precursor. Subsequently, 0.45 g of thiourea (99%, Sigma-Aldrich) was added to the PTA solution. The PTA/thiourea precursor was stirred to remove the solvent until the weight of the solution was 3.5 g. The PTA/thiourea solution was spun onto FTO-coated glass (Solaronix) followed by heat treatment at 400 °C for 30 min. As shown in step ii in Figure 1a, the Al metal lines were locally deposited on the tungsten oxide film by sputtering through a shadow mask. The active area of the resistive switching region, i.e. Al/WO_x/FTO RRAM units, is 1.6 mm^2. Subsequently, the Al(patterned)/WO_x/FTO-glass and ITO-glass were sandwiched using 60 μm thick hot-melt Surlyn spacers (Solaronix). The electrolyte solution of 1 M lithium percholorate ($LiClO_4$, Sigma-Aldrich) in propylene carbonate (PC, Alfa Aesar) was introduced between Al(patterned)/WO_x and the ITO counter electrode by capillary action to form the EC unit (step iii in Figure 1a). A schematic of the WO_x-based device composed of EC and RRAM units is shown in Figure 1b.

The cross-sectional microstructures of Al/WO_x/FTO-glass sample were investigated using field-emission transmission electron microscopy (TEM, JEOL JEM-2100F CS STEM) and chemical bonding state of the WO_x film was examined using X-ray photoelectron spectroscopy (XPS, PHI 5000 VersaProbe). The coloration efficiency and transmittance of the EC unit were obtained using a Si photodetector (model 71640, Newport) and a red laser module (M&T OPTICS, Taiwan) (intensity: 3.8 mW; wavelength: 650 nm) when intercalating/extracting Li ions at a constant current density of 1 $mAcm^{-2}$ (controlled using a Keithley 2400 sourcemeter).[3] The resistive switching behavior of the Al/WO_x/FTO RRAM units is characterized using a precision semiconductor parameter analyzer (Agilent 4156C) with a sweeping voltage applied to the Al top-electrode while the FTO bottom-electrode was ground. The current−voltage ($I-V$) measurement apparatus is set in a metal dark box to prevent the disturbance of light and electromagnetic waves.

3. RESULTS AND DISCUSSION

Figure 2a shows the cross-sectional TEM bright-field (BF) image of the Al/WO_x/FTO structure. This micrograph reveals the thicknesses of the Al top-electrode and WO_x layer (100 and 370 nm, respectively) and some lightly contrasted, drop-like features in WO_x. The microstructure of WO_x is further unveiled with a magnified scanning TEM (STEM) BF image, as shown in Figure 2b. The image shows dark-contrasted grains with a size of ~5−10 nm and white-contrasted speckles with a size of ~15 nm scattered in the WO_x layer. Due to the porous nature of our thiourea-assisted WO_x film,[3] we suggest that the lightly contrasted drop-like features and white speckles in a and b in Figure 2, respectively, are pores. On the contrary, the dark-contrasted grains in Figure 2b shall be related to materials whose chemical composition is heavier than that of the WO_x matrix; these grains are more concentrated near the Al/WO_x interface than inside the film.

To qualitatively perceive the compositional differences in the WO_x layer, Figure 2c shows a high-angle annular dark-field STEM (HAADF-STEM) image of the Al/WO_x interface. The contrast in the HAADF-STEM micrographs is strongly correlated with the atomic mass of the imaged region: heavier elements contributing to the brighter contrast and vice versa. The HAADF-STEM image of WO_x in Figure 2c contains dark- and bright-contrasted regions embedded in a gray matrix. The dark-contrasted area represents the low-atomic-mass regions, which shall be related to the pores in WO_x and correspond to the lightly contrasted, droplike features shown in Figure 2a, as well as the white-contrasted speckles in Figure 2b. On the other hand, because the atomic mass of W is much heavier than that of O, the bright-contrasted clusters with a size of ~5−10 nm in the WO_x HAADF-STEM image of Figure 2c should correspond to the dark-contrasted grains revealed in the BF STEM image of Figure 2b, both suggesting a tungsten(W)-rich composition in these clusters (or grains). These clusters are not only scattered within the WO_x layer but also concentrated along the interface between the Al top-electrode and the WO_x film, which is involved in the formation of conductive paths during resistive switching and will be discussed later. In addition, the chemical element analysis of Al/WO_x/FTO-glass sample has been carried out by energy dispersive X-ray spectrometry (EDX) combined with the STEM. Figure S1 (see the Supporting Information) shows the EDX spectra obtained from the WO_x layer and the interfacial region between Al electrode and WO_x layer of Al/WO_x/FTO sample. In Figure S1a in the Supporting Information, the intensity of oxygen signal (at ~0.52 keV) from WO_x layer is about 75% of that of tungsten

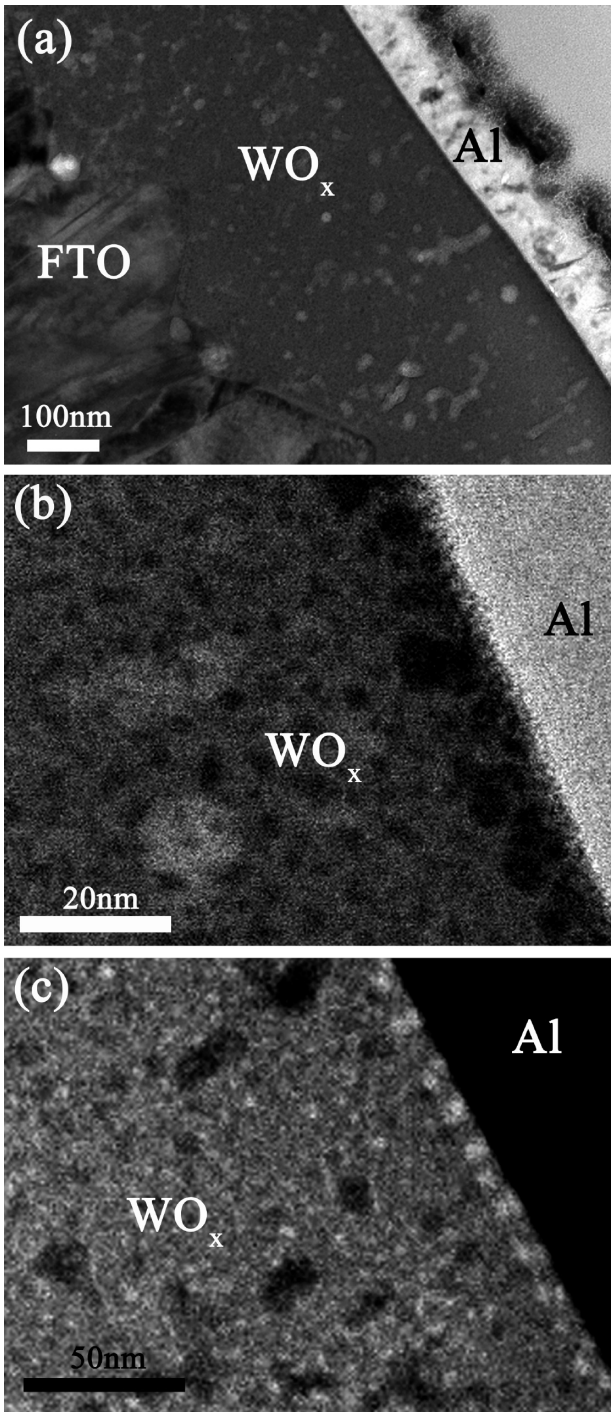

Figure 2. Cross-sectional (a) TEM BF and (b) STEM BF images of Al/WO_x/FTO sample. (c) HAADF-STEM image of Al/WO_x/FTO sample.

signal (at ~8.39 keV). In contrast, the oxygen/tungsten intensity ratio is less than 25% in the interface region (where the nanoclusters are abundant), as shown in Figure S1b in the Supporting Information. Because of the nanoclusters are in spherical shape and embedded in oxide matrix, the oxygen signal from the oxide matrix will also be detected in the interfacial regions. However, because of the relatively weak peak intensity (see Figure S1b in the Supporting Information), the nanoclusters in the interfacial region shall be rich in metallic-W.

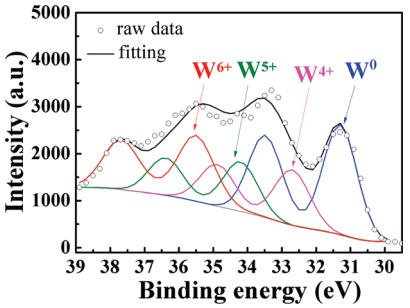

Figure 3. W 4f core level XPS spectrum taken from the WO_x film. The spectrum is deconvoluted into $W4f_{7/2}$ and $4f_{5/2}$ doublets associated with W^0, W^{4+}, W^{5+}, and W^{6+} configurations.

The chemical bonding state in the WO_x film was further examined using XPS. The W4f XPS spectrum is depicted in Figure 3. The spectrum has been calibrated for the charge effect with reference to the C1s peak at 284.5 eV.[21] The W4f spectrum was deconvoluted into four pairs of W4f doublet peaks pertaining to four tungsten oxidation states: W^0, W^{4+}, W^{5+}, and W^{6+}. The $W4f_{7/2}$ peaks associated with W^0, W^{4+}, W^{5+}, and W^{6+} are located at 31.3, 32.7, 34.2, and 35.6 eV, respectively.[21−24] Multiple W−O bonding states, i.e., W^{4+}, W^{5+}, and W^{6+} oxidation states, are observed, which implies that a substantial amount of oxygen vacancies exits in the WO_x layer. Some of W atoms are in the metallic state (i.e., W^0). The integrated intensity for W XPS signals of different oxidation states has been calculated from Figure 3. A substantial W^0 peak area of ~37.6% exists in our WO_x layer, which is much greater as compared to that in the monoclinic film[25] and it suggests a significant quantity of metallic W atoms (in W^0 state) exists. Accordingly, the presence of the W^0 state in XPS spectrum and the rich W content at the interfacial region observed in EDX analysis confirm that the heavy-element, nanosized grains observed in the TEM micrographs are composed of metallic-W nanoclusters.

The modulation of transmittance for the EC unit, i.e., FTO-glass/WO_x/electrolyte/ITO-glass, is founded on the EC performance of WO_x upon current injection through the ITO-counter electrode. An EC material with a high coloration efficiency can provide a large transmittance modulation via a small change in the number of intercalated cations, which might result in good cycling reversibility due to the low charge needed for coloration. Figure 4a shows a plot of optical density (O.D.) versus injected charge density (Q) of the EC unit during the intercalation of Li ions at a constant current density of 1 $mAcm^{-2}$. The coloration efficiency is estimated to be 40 cm^2C^{-1} from the slope of O.D. to Q. The coloration efficiency is comparable to those of nanocrystalline,[2] thermally evaporated[26] and nanobundle[27] films. When the injected charge densities, i.e., the quantities of intercalated Li ions, are set at 0, 2, 5, 10, and 20 $mCcm^{-2}$, the transmittances and associated photographs are shown in Figure 4b. As the number of injected Li ions increases, the EC unit becomes cyan, blue, and navy blue in sequence. The colored EC unit bleaches to a transparent state after a complete extraction of intercalated Li ions (i.e., when the total injected charge returns to 0 $mCcm^{-2}$). Time evolution of the transmittance of the EC unit with different quantities of intercalated Li ions in the WO_x layer is shown in Figure S2 (see the Supporting Information). It reveals that the transmittance of the EC unit is sustained within ±3% deviation for a retention time of 1800 s, indicating the existence of nonvolatile transmittance-states of the

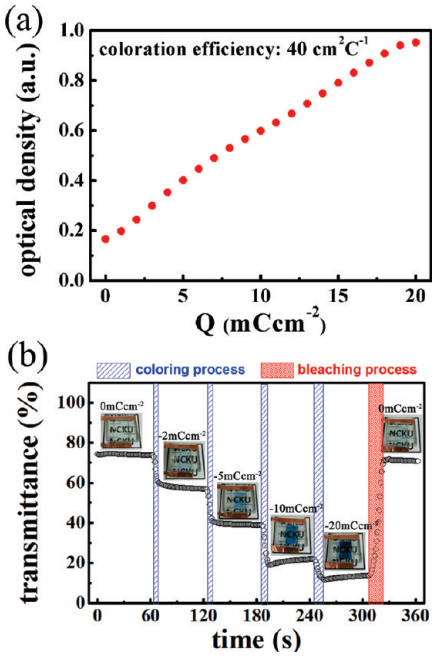

Figure 4. (a) Optical density versus intercalated charge densities for the EC unit during the intercalation of Li ions at a constant current density of 1 mA cm^{-2}. The coloration efficiency estimated from the slope of this curve is 40 cm^2 C^{-1}. (b) The time-dependent transmittance regulation and corresponding photographs with different quantities of intercalated Li ions in the WO_x layer of the EC unit (the blue slash region and red crisscross region indicate the progressions of coloring and bleaching, respectively).

device. The slight divergence of the transmittance always occurs in the early stage of the retention time measurement as shown in Figure S2 in the Supporting Information. After the extraction/intercalation of Li ions with applied current, it will take a short period of time to reach the compositional homogeneity of WO_x/Li_yWO_x layer by diffusion of the Li ions at open circuit.[28] Consequently, a slight divergence of the transmittance is detected in the beginning of the retention measurement. After the retention test shown in Figure S2 in the Supporting Information, the same device was switched between multiple-states for several times. Although multiple states are still demonstrated, the transmittances of the WO_x layers with various amounts of Li intercalation are different from those recorded in Figure 4b. It indicates that the reversibility of the EC unit is not good in the present version of the device due to the formation of bubbles by electrochemical reaction with the electrolyte. In addition, the ITO counter electrode of EC unit becomes opaque at a large applied voltage, which decreases the transmittance of the device as well after several intercalation/extraction processes. We suggested that the issues may be solved by employing another suitable electrolyte and FTO counter electrode in the EC unit. It should also be noted that the nanosized pores in WO_x not only increase the surface area but also provide channels for electrolyte to enfold WO_x, decreasing the needed diffusion distance for Li ions.[1−3] Therefore, the pores in WO_x promote ion-intercalation kinetics and are critical to EC performance. Accordingly, the EC unit possesses multiple transmittance states that depend on degree of intercalation/extraction of Li ions, which is similar to those of EC polymeric memory devices which record data based on variations in transmittance.[9,10]

The current−voltage (I−V) characteristic curves in Figure 5a reveal the bipolar resistive switching character of the solution-processed WO_x RRAM unit. The Al/WO_x/FTO RRAM unit initially exhibits a high-resistance state (HRS) and is switched to a low-resistance state (LRS) at a threshold voltage of −5.2 V, as illustrated in step 1 of Figure 5a. The LRS current is limited by a compliance value of 10 mA to prevent permanent dielectric breakdown. Once the negative bias sweep is again applied to the Al top-electrode, the I−V curve (step 2) reveals that the RRAM unit remains at the LRS. Subsequently, the RRAM unit is switched back to the HRS after a positive bias sweep is applied, as shown in step 3. The RRAM unit remains in the HRS under a subsequent negative bias (applied to the Al electrode) sweep until the threshold voltage is reached, as displayed in step 4. Therefore, the RRAM unit exhibits bipolar resistive switching behavior. Since electrical stability is an important issue for NVM, the RRAM units at LRS and HRS have been examined using a retention test under a constant readout voltage of 0.1 V. As shown in Figure 5b, both the LRS and HRS are well maintained over 12000 s in the retention test, confirming the nonvolatile nature of the resistive switching behavior. The resistance ratio of the HRS to the LRS can be as high as 1×10^4 (1×10^2 to 1×10^4 in general). In addition, good endurance is the fundamental challenge for NVM and electric-pulse-induced resistive switching measurements of our RRAM units are conducted. Figure S3 (see the Supporting Information) shows the nondegradable endurance characteristics of RRAM units and acceptable electrical endurance of 100 cycles is obtained. Therefore, WO_x-based RRAM units possess the bipolar resistive switching behavior with acceptable retention and endurance characteristics, which are suitable for the NVM application and comparable to those of previously reported tungsten oxide-based RRAM devices.[15,16]

The resistive switching of our RRAM unit shall be associated with the formation of filament-like conductive paths in the oxide layer (via the alignment of defects)[20] or the dynamic filament terminal,[29,30] but unlikely originated from change of Schottky barrier width at the interface between the electrode and oxide,[31] because of the area-independence of resistances for the HRS and LRS in our RRAM unit (see Figure S4 in the Supporting Information). However, the switching polarity of our RRAM unit is the exact opposite of the model with dynamic filament terminal (in which a negative bias shall be applied to the nonohmic electrode (i.e., the FTO electrode in our case)). Therefore, the dynamic filament terminal model may not be applicable to our RRAM unit and the resistive switching of our RRAM device shall be related to the construction of conductive paths based on moving and aggregation of oxygen vacancies.

To elucidate the resistive switching mechanism, we present a schematic drawing in Figure 5c, where the thickness of the WO_x layer is enlarged for clarity. Because W atoms in the WO_x film of our RRAM units are in the form of multiple oxidation states, as revealed by TEM and XPS analyses (Figure 2 and Figure 3), there will exist substantial number of metallic W clusters and oxygen vacancies (as shown in the pristine panel of Figure 5c). It has been reported that metallic nanocrystals embedded in semiconductors and/or insulators produce a localized enhanced electric field along the direction of externally applied electric field, no matter the metallic nanocrystals are distributing in parallel with or perpendicularly to the electrodes.[32−34] Accordingly, the metallic-W nanoclusters embedded in the WO_x layer shall play a key role in the electric field enhancement, which promotes the aggregation (i.e., local alignment) of oxygen

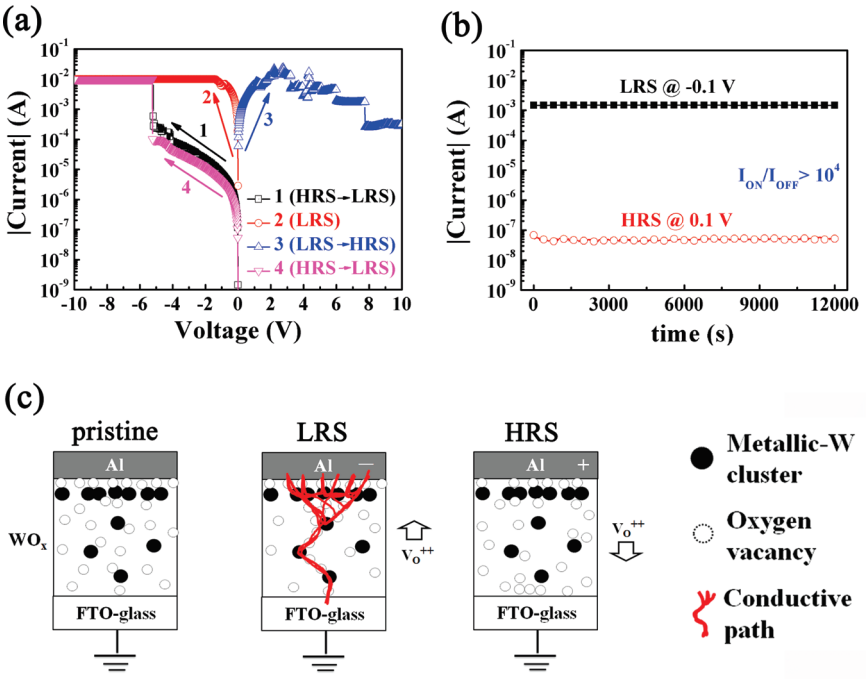

Figure 5. (a) $I-V$ characteristics of the Al/WO_x/FTO RRAM unit (the current compliance of the LRS is set at 10 mA). (b) Retention test for the LRS and the HRS of the RRAM unit under a continuous 0.1 V readout voltage. Both LRS and HRS are maintained the retention data for over 12 000 s. The LRS/HRS current ratio is more than 1×10^4. (c) Schematics for bipolar resistive switching mechanism of the Al/WO_x/FTO RRAM unit (thickness of WO_x is enlarged for clarification).

vacancies between metallic-W nanoclusters. In addition, the metallic-W nanoclusters gathered along the interface between the Al electrode and WO_x film are possibly related with the reduction of WO_x by Al owing to the thermodynamic driving force[35] and it shall be accompanied with the generation of oxygen vacancies (as shown in pristine panel of Figure 5c).

The conducting paths formed by aggregation of oxygen vacancies generally exhibit a conical shape, with a wider diameter at the negatively biased electrode.[36−38] The bipolar switching polarity (negative-ON/positive-OFF with respect to the Al electrode) is associated with the rich oxygen vacancies near the Al/WO_x interface, which plays a decisive role in the formation of conductive paths. As illustrated in the LRS panel of Figure 5c, the rich oxygen vacancies near the Al/WO_x interface provide the "broad base" for the conducting paths. A negative voltage applied to Al electrode of our RRAM unit attracts the positively charged oxygen vacancies. The aggregation of oxygen vacancies between metallic-W clusters forms a cone-shaped path that electrically connects the top and bottom electrodes in the RRAM unit.[39,40] As a result, the RRAM unit of the WO_x-based device is switched to the LRS.

To switch the RRAM unit back to the HRS, a positive bias on the Al top-electrode is needed, as shown in the HRS panel of Figure 5c. Under this bias polarity, oxygen vacancies are repelled away from the Al/WO_x interface. The vacancies are driven to the WO_x/FTO interface; however, it is difficult to construct a conical conductive path with a larger diameter at the WO_x/FTO interface because the quantity of oxygen vacancies is rather limited around the FTO electrode. Consequently, the conductive paths are ruptured and the RRAM unit is switched back to the HRS. Note that the RRAM unit cannot switch from the HRS to the LRS when the applied voltage to the Al electrode is positive, even when it is up to +30 V. Similar to the situation drawn in the HRS panel of Figure 5c, the positive bias on Al electrode drives oxygen vacancies to the FTO electrode but it is difficult to build a continuous, conductive path of conical shape with a broad diameter at the WO_x/FTO interface. As a result, the RRAM unit cannot be switched on under this polarity.

4. CONCLUSION

We have synthesized WO_x films via a thiourea-assisted route. A WO_x-based device composed of Al(patterned top electrode)/WO_x/FTO(bottom electrode) RRAM and FTO/WO_x/electrolyte/ITO EC units is demonstrated. The EC unit possesses multiple transmittance states depending on the quantity of intercalated Li ions in the WO_x films. On the other hand, the RRAM unit exhibits bipolar resistive switching behavior with an ON/OFF current ratio of more than 1×10^4. Cross-sectional TEM images reveal that the WO_x film contains nanosized pores and metallic-W nanoclusters embedded in the tungsten oxide matrix. Multiple W−O bonding states are observed in the W 4f XPS spectrum, which implies the existence of oxygen vacancies in the WO_x layer. In addition, some metallic-W nanoclusters are concentrated along the interface between the Al electrode and WO_x film, which shall be accompanied with a substantial amount of oxygen vacancies near the Al/WO_x interface. The nanosized pores in the WO_x film facilitate the transport of Li ions for the modulation of transmittance, while the metallic-W clusters enhance the local electric field for the aggregation of oxygen vacancies. Furthermore, the rich oxygen vacancies near the Al/WO_x interface play a decisive role in the formation/rupture of cone-shaped conductive paths during bipolar resistive switching. As a result, the specific microstructure of thiourea-assisted WO_x film brings forth the multiple EC states and resistive switching behavior, which may be implemented to optical and electrical nonvolatile data storage devices, respectively.

■ ASSOCIATED CONTENT

Supporting Information. Figures of material analysis including EDX spectra of Al/WO_x/FTO sample (Figure S1), nonvolatile transmittance states of the EC units (Figure S2), endurance performance of RRAM units (Figure S3) and area dependence of resistance values in HRS and LRS for WO_x-based RRAM units (Figure S4). This material is available free of charge via the Internet at http://pubs.acs.org/.

■ AUTHOR INFORMATION

Corresponding Author

*E-mail: jenschen@mail.ncku.edu.tw. Tel.: +886-6-2757575, ext. 62948, Fax: +886-6-2762541. Address: No.1, University Road, Tainan City 701, Taiwan.

■ ACKNOWLEDGMENT

The authors gratefully acknowledge the financial support from the National Science Council of Taiwan (Grants NSC-96-2628-E-006-013-MY3 and NSC-100-3113-E-006-004), NCKU Landmark Project (A0051) and Applied Materials Taiwan.

■ REFERENCES

(1) Granqvist, C. G. *Handbook of Inorganic Electrochromic Materials*; Elsevier: The Netherlands, 1995.
(2) Lee, S. H.; Deshpande, R.; Parilla, P. A.; Jones, K. M.; To, B.; Mahan, A. H.; Dillon, A. C. *Adv. Mater.* **2006**, *18*, 763–766.
(3) Wu, W. T.; Liao, W. P.; Chen, J. S.; Wu, J. J. *ChemPhysChem* **2010**, *11*, 3306–3312.
(4) Rossinyol, E.; Prim, A.; Pellicer, E.; Arbiol, J.; Hernandez - Ramirez, F.; Peiro, F.; Cornet, A.; Morante, J. R.; Solovyov, L. A.; Tian, B. Z.; Bo, T.; Zhao, D. Y. *Adv. Funct. Mater.* **2007**, *17*, 1801–1806.
(5) Chen, D.; Ye, J. H. *Adv. Funct. Mater.* **2008**, *18*, 1922–1928.
(6) Baetens, R.; Jelle, B. P.; Gustavsen, A. *Sol. Energy Mater. Sol. Cells* **2010**, *94*, 87–105.
(7) Tajima, K.; Yamada, Y.; Bao, S.; Okada, M.; Yoshimura, K. *Appl. Phys. Lett.* **2008**, *92*, 041912.
(8) Monk, P. M. S.; Mortimer, R. J.; Rosseinsky, D. R. *Electrochromism: Fundamentals and Applications*; VCH: Weinheim, Germany, 1995.
(9) Sonmez, G.; Sonmez, H. B. *J. Mater. Chem.* **2006**, *16*, 2473–2477.
(10) de Ruiter, G.; Wijsboom, Y. H.; Oded, N.; van der Boom, M. E. *ACS Appl. Mater. Interfaces* **2010**, *2*, 3578–3585.
(11) Lee, M. J.; Han, S.; Jeon, S. H.; Park, B. H.; Kang, B. S.; Ahn, S. E.; Kim, K. H.; Lee, C. B.; Kim, C. J.; Yoo, I. K.; Seo, D. H.; Li, X. S.; Park, J. B.; Lee, J. H.; Park, Y. *Nano Lett.* **2009**, *9*, 1476–1481.
(12) Seo, S.; Lee, M. J.; Seo, D. H.; Jeoung, E. J.; Suh, D. S.; Joung, Y. S.; Yoo, I. K.; Hwang, I. R.; Kim, S. H.; Byun, I. S.; Kim, J. S.; Choi, J. S.; Park, B. H. *Appl. Phys. Lett.* **2004**, *85*, 5655–5657.
(13) Xia, Q. F.; Yang, J. J.; Wu, W.; Li, X. M.; Williams, R. S. *Nano Lett.* **2010**, *10*, 2909–2914.
(14) Yang, J. J.; Miao, F.; Pickett, M. D.; Ohlberg, D. A. A.; Stewart, D. R.; Lau, C. N.; Williams, R. S. *Nanotechnology* **2009**, *20*, 215201.
(15) Ho, C. H.; Hsu, C. L.; Chen, C. C.; Liu, J. T.; Wu, C. S.; Huang, C. C.; Hu, C. M.; Yang, F. L. *IEEE International Electron Devices Meeting, San Francisco* **2010**, 10–436.
(16) Shang, D. S.; Shi, L.; Sun, J. R.; Shen, B. G.; Zhuge, F.; Li, R. W.; Zhao, Y. G. *Appl. Phys. Lett.* **2010**, *96*, 072103.
(17) Yao, J.; Sun, Z. Z.; Zhong, L.; Natelson, D.; Tour, J. M. *Nano Lett.* **2010**, *10*, 4105–4110.
(18) Szot, K.; Speier, W.; Bihlmayer, G.; Waser, R. *Nat. Mater.* **2006**, *5*, 312–320.
(19) Moreno, C.; Munuera, C.; Valencia, S.; Kronast, F.; Obradors, X.; Ocal, C. *Nano Lett.* **2010**, *10*, 3828–3835.
(20) Waser, R.; Dittmann, R.; Staikov, G.; Szot, K. *Adv. Mater.* **2009**, *21*, 2632–2663.
(21) Moulder, J. F.; Stickle, W. F.; Sobol, P. E.; Bomben, K. D. *Handbook of X-ray Photoelectron Spectroscopy*; Chastain, J., King, R. C., Eds.; Physical Electronics Inc.: Eden Prairie, MN, 1995.
(22) Sohal, R.; Walczyk, C.; Zaumseil, P.; Wolansky, D.; Fox, A.; Tillack, B.; Mussig, H. J.; Schroeder, T. *Thin Solid Films* **2009**, *517*, 4534–4539.
(23) Manning, T. D.; Parkin, I. P. *J. Mater. Chem.* **2004**, *14*, 2554–2559.
(24) Senthil, K.; Yong, K. *Nanotechnology* **2007**, *18*, 395604.
(25) Bathe, S. R.; Patil, P. S. *Solid State Ion.* **2008**, *179*, 314–323.
(26) Kaneko, H.; Nishimoto, S.; Miyake, K.; Suedomi, N. *J. Appl. Phys.* **1986**, *59*, 2526–2534.
(27) Yoo, S. J.; Lim, J. W.; Sung, Y. E.; Jung, Y. H.; Choi, H. G.; Kim, D. K. *Appl. Phys. Lett.* **2007**, *90*, 173126.
(28) Weppner, W.; Huggins, R. A. *J. Electrochem. Soc.* **1977**, *124*, 1569–1578.
(29) Yang, J. J.; Pickett, M. D.; Li, X. M.; Ohlberg, D. A. A.; Stewart, D. R.; Williams, R. S. *Nat. Nanotechnol.* **2008**, *3*, 429–433.
(30) Miao, F.; Yang, J. J.; Strachan, J. P.; Stewart, D.; Williams, R. S.; Lau, C. N. *Appl. Phys. Lett.* **2009**, *95*, 113503.
(31) Sawa, A. *Mater. Today* **2008**, *11*, 28–36.
(32) Zuo, Q. Y.; Long, S. B.; Liu, Q.; Zhang, S.; Wang, Q.; Li, Y. T.; Wang, Y.; Liu, M. *J. Appl. Phys.* **2009**, *106*, 073724.
(33) Chang, W. Y.; Cheng, K. J.; Tsai, J. M.; Chen, H. J.; Chen, F.; Tsai, M. J.; Wu, T. B. *Appl. Phys. Lett.* **2009**, *95*, 042104.
(34) Prime, D. C., *Switching Mechanisms, Electrical Characterisation and Fabrication of Nanoparticle Based Non-Volatile Polymer Memory Devices*, Ph. D. thesis, De Montfort University, Leicester, U.K., 2010; pp 119
(35) Barin, I. *Thermochemical Data of Pure Substances*; VCH: New York, 1995.
(36) Kwon, D. H.; Kim, K. M.; Jang, J. H.; Jeon, J. M.; Lee, M. H.; Kim, G. H.; Li, X. S.; Park, G. S.; Lee, B.; Han, S.; Kim, M.; Hwang, C. S. *Nat. Nanotechnol.* **2010**, *5*, 148–153.
(37) Kim, K. M.; Hwang, C. S. *Appl. Phys. Lett.* **2009**, *94*, 122109.
(38) Lee, J.; Bourim, E.; Lee, W.; Park, J.; Jo, M.; Jung, S.; Shin, J.; Hwang, H. *Appl. Phys. Lett.* **2010**, *97*, 172105.
(39) Cao, X.; Li, X. M.; Gao, X. D.; Yu, W. D.; Liu, X. J.; Zhang, Y. W.; Chen, L. D.; Cheng, X. H. *J. Appl. Phys.* **2009**, *106*, 073723.
(40) Pan, T. M.; Chen, K. M.; Lu, C. H. *Electrochem. Solid-State Lett.* **2011**, *14*, H27–H29.